Journal of Materials Chemistry

Cite this: *J. Mater. Chem.*, 2011, **21**, 12381

www.rsc.org/materials

PAPER

Amphiphilically-modified gelatin nanoparticles: Self-assembly behavior, controlled biodegradability, and rapid cellular uptake for intracellular drug delivery

Wei-Ming Li, Dean-Mo Liu* and San-Yuan Chen*

Received 13th January 2011, Accepted 31st May 2011
DOI: 10.1039/c1jm10188a

An amphiphilic gelatin macromolecule capable of self-assembling to form micelle-like nanospheres for entrapping hydrophobic therapeutic molecules was successfully synthesized by grafting hydrophobic hexanoyl anhydrides to the amino groups of primitive gelatin. The substitution and grafting efficiency of the modified gelatin displayed a concentration-dependent manner toward the hexanoyl anhydride. The particle size and stability of the resulting self-assembled nanoparticles strongly depend on the degree of substitution of the gelatin. These gelatin nanoparticles exhibited an outstanding cytocompatibility and highly efficient drug encapsulation efficiency. The drug release profile of the anticancer agent (camptothecin) from the amphiphilic gelatin nanoparticles shows that the drug release mechanism is dominated by a combined effect of diffusion and degradation. Furthermore, a tunable sustained release and degradation behavior can be controlled by changing the degree of substitution of the gelatin. This new type of amphiphilic gelatin nanoparticles with controlled biodegradability and rapid cellular internalization may serve in the intracellular delivery of specific proteins or genes, permitting a novel design for intracellularly-based nanotherapy.

Introduction

Intracellular drug delivery systems have recently received significant attention for their potential clinical capabilities for efficient targeting and up-take by diseased cells over conventional systemic drug delivery systems.[1] However, to achieve such a therapeutic strategy in the nano scale, vehicles of controlled drug delivery require design at the molecular level and subtle manipulation of the delivery systems to function effectively during the course of medication. Ideal nanovehicles should have improved biocompatibility,[2] tunable biodegradability,[3] optimal size for cellular internalization,[4] high drug payload, extended circulation time, be capable of accumulating at targeted sites in the body,[5,6] and deliver effective medication with minimal side effects to patients. Numerous biocompatible materials including natural polymers,[7] synthetic polymers,[8] oxides, carbon derivatives,[9] lipids,[10] and hybrids have been developed to date, and some of them have received considerable successes from *in vivo* to clinical practices in the past. Among them, polymeric biomaterials including block copolymers, micelles, liposomes and natural polymers have been recognized as major players in the development of drug delivery systems in recent decades. Each one of these systems has been designed to provide hydrophobic micro-domains in aqueous solutions, which can accommodate a hydrophobic cargo. For instance, polymeric micelles composed of block copolymers have been intensively investigated as drug delivery vehicles because of their tunable particle size, thermodynamic stability, ability to dissolve hydrophobic molecules, protection of bioactive molecules and minimal adverse side effects. Among those polymer-based delivery systems, natural polymers have been one of the most exciting systems to explore, because they represent the group of materials most abundantly present on this planet and least detrimental to the environment and the human body. Polysaccharides are important biological candidates because they are highly biocompatible, biodegradable, and less harmful to humans than are other candidates. The use of polysaccharides for biological applications has long been studied in a range of environments from *in vitro* conditions to clinical practice dating back for a century. However, with the development of advanced chemical synthesis and biomaterials technology, chemical or biological modifications of polysaccharides have received wide-spread attention because the newly formed polysaccharide molecules can be functionalized for a variety of biomedical purposes, such as drug/gene/protein delivery,[3] wound dressing, and tissue engineering. However, the development of a functionalized protein for biomedical uses is less emphasized in literature, possibility due to its vulnerability as a result of denaturation. Hydrophobic modification of proteins or protein-like macromolecules such as gelatin is expected to bring numerous new contributions to such fields as biomedicine,

Department of Materials Sciences and Engineering, National Chiao Tung University, Hsinchu, 30010, Taiwan. E-mail: sanyuanchen@mail.nctu.edu.tw; deanmo_liu@yahoo.ca

pharmaceutics, and tissue engineering due to its inherently excellent biodegradability and biocompatibility. Therefore, the main goal of this investigation is to systematically design and study a chemically modified gelatin. Gelatin is a natural polymer obtained by partial hydrolysis of collagen and the reactive amino groups in the backbones of gelatin. This structure makes it possible to chemically conjugate gelatin with various organic molecules to form an amphiphilic entity. The hydrophobically modified gelatin is also expected to self-assemble for drug encapsulation.[11,12] A potential advantage of using such a protein-based carrier is the ease of sequence modification and design to allow cell penetration and active targeting. Here, we employ a small, linear aliphatic ligand, *i.e.*, hexanoyl groups, to modify the amino groups along the fibrous gelatin scaffold to form amphiphilic gelatin. This modification is intended to impart a hydrophobic property to the gelatin molecule with no influence on its molecular flexibility. The major goal of this investigation is to gain a better understanding on the chemical and biological properties of the amphiphilic gelatin by exploring the self-assembly behavior, drug encapsulation/release, degradation, and cytocompatibility of the resulting gelatin nanoparticles.

Materials and methods

Material

Gelatin type A, bloom 300 (Mw 87.5 KDa), hexanoic anhydride, picrylsulfonic acid, pyrene, sodium hydroxide, camptothecin (CPT), fluorescein isothiocyanate (FITC), ethanol, and a dialysis tubing cellulose membrane (MWCO: 12,400 and 2,000) were obtained from Sigma Chemical Co. Human retinal pigmented epithelium cell (ARPE-19) was obtained from the Bioresource Collection and Research Center in Taiwan. All other reagents were of analytical grade.

Preparation of amphiphilic gelatin molecules

Gelatin in the amount of 1.25 g was taken up in 20 mL of water, and the suspension was gently mixed with 2 mL of 0.1 N NaOH solution and stirred for 0.5 h at 70 °C. Subsequently, 2, 4, 6, and 8 mL of hexanol anhydride was added to 20 mL of gelatin solution, stirred at 70 °C, and designated as GM1, GM2, GM3, GM4, respectively. After a reaction time of 5 h, the mixture was cooled to room temperature and the pH was adjusted to 7.4 with diluted sodium hydroxide. The resulting solutions were collected by a dialysis tubing cellulose membrane after dialysis with ethanol solution (25% v/v) for 24 h. The gel was then dried in the oven at 60 °C and ground to a powder to store in vials.

Characterization of amphiphilic gelatin molecules

The ^{1}H NMR spectra of the amphiphilic gelatin molecules were obtained using a 500-MHz NMR (VARIAN, UNIYTINOVA-500 NMR). ^{1}H NMR spectra were also obtained separately in 0.5 wt % D_2O to characterize the structure of the amphiphilic gelatin molecules. IR spectra were obtained with attenuated total reflectance Fourier transformed infrared (ATR-FTIR) spectroscopy and recorded on a spectrometer (Bomem DA8.3, Canada).

Quantification of free amino group content

The self-assembled nanoparticles were dispersed in water (0.73 mg mL^{-1}), and 500 μL of the solution was diluted with the same volume of water. 1 mL of 4% sodium hydrogen carbonate solution (with a pH of 8.5) and 1 mL of aqueous 0.1% TNBS solution were added to the nanoparticle dispersion. The mixture was stirred at 250 rpm for 2 h at 37 °C and centrifuged at 13,000 × g for 30 min to collect the nanoparticles. The resulting supernatant (560 μL) was diluted with 1 mL water and quantified for the unreacted TNBS with a UV/VIS spectrophotometer (Agilent, 84531 UV-Visible spectrophotometer) at 350 nm. The content of amino groups in the self-assembled nanoparticles was calculated relative to a TNBS reference containing water and primitive gelatin.

Measurement of critical aggregation concentration (CAC)

The CAC was determined using pyrene as a fluorescence probe. Pyrene was first dissolved in acetone, and then added to deionized water to a concentration of 5×10^{-7} M. Acetone was subsequently removed by reducing the atmospheric pressure to allow its evaporation and stirring for more than 5 h at 37 °C. The concentration of self-assembled gelatin nanoparticles in the water varied from 0.0001 to 0.1 g L^{-1}. Prior to measurement, the pyrene and self-assembled nanoparticles in the water were conjugated and equilibrated at room temperature for 1 day. The fluorescence spectra were obtained at room temperature using a fluorescence spectrophotometer (Hitachi FL-4500, Japan).

Characterization of self-assembled gelatin nanoparticles

The effective hydrodynamic diameter of the self-assembled nanoparticles was measured at 25 °C with a Zetasizer 3000ES (Malven Instruments, Malvern, U.K.) and a 670 nm wavelength argon laser beam with a detector angle of 90°. Morphological evaluation of the self-assembled nanoparticles was performed by transmission electron microscopy (TEM) (JEOL2100, Japan) and scanning electron microscopy (SEM) (S6500, JEOL, Japan).

Drug loading efficiency of self-assembled nanoparticles

Self-assembled nanoparticles preloaded with drugs were prepared by dissolving 20 μg mL^{-1} of camptothecin (CPT) in 20 mL nanoparticle suspension acquired before ultrasonication. Insoluble, free CPT was removed by centrifugation at 12000 rpm and 4 °C for 10 min. The drug-containing nanoparticles were then separated from the aqueous solution by centrifugation at 15000 rpm and 4 °C for 15 min. The drug concentration in the supernatant was analyzed using ultraviolet absorption (UV) at a wavelength of 366 nm, a strong absorption band of CPT, with reference to a calibration curve on a UV-Vis spectrometer (Agilent, 84531 UV-Visible spectrophotometer). The encapsulation efficiency (EE) was obtained using the following equation:

$$EE = (L_1 - L_2)/L_1 \times 100$$

Where L_1 is the total amount of the CPT, and L_2 is the amount of CPT remaining in the supernatant.

Release of drug from self-assembled nanoparticles

A solution of CPT or CPT-loaded nanoparticles (20 μg mL^{-1} CPT equiv) was added to a dialysis tubing cellulose membrane with a cut-off molecular weight of 12 400. The solution was dialyzed at 37 °C against simulated body fluid (SBF). The solution was removed periodically from the dialysis tubing to measure its absorbance spectra at a wavelength of 366 nm and to determine the amount of CPT in the solution. The solution was maintained at a constant volume by replacing original solution with fresh media.

Degradation test

The degradation test was performed using the same method for the drug release test as described in section 2.8. The small molecular weight of the dialysis tubing cellulose membrane was used to determine the amount of degradant generated in the medium. A solution of amphiphilic gelatin was added to a dialysis tubing cellulose membrane with a cut-off molecular weight of 2,000. The solution was dialyzed at 37 °C against SBF. The absorbance of the solution was measured at a wavelength of 280 nm to determine the amount of degraded gelatin.

Cell viability

A comparison of the *in vitro* cytotoxicity of self-assembled nanoparticles with different concentrations was performed on ARPE-19 cells using an *in vitro* proliferation method and MTT. Briefly, 1×10^4 cells $well^{-1}$ were plated in 96-well plates and exposed to the serial concentrations of self-assembled nanoparticles at 37 °C for 24 h. Subsequently, 20 mL of MTT solution (5 mg mL^{-1} in PBS, pH 7.4) was added, and the cells were incubated for an additional 4 h. Then the medium was replaced with 200 mL of DMSO and the absorbance was monitored using a Sunrise absorbance microplate reader at the dual wavelengths of 595 nm. In addition, ARPE-19 cells were seeded on 96-well plates at a density of 5×10^3 cells $well^{-1}$ and incubated for 24 h. After incubation, the medium was replaced with 200 μL of fresh medium containing nanoparticles with a concentration of 500 μg mL^{-1} and incubated again for different times. After incubation, 20 μL of MTT solution was added and the cells were incubated for another 4 h. Finally, the cell viability was performed using the same method. Cell viability was determined by comparison with untreated cells and calculated according to the following equation:

$$\text{Cell viability (\%)} = (A_{\text{sample}}/A_{\text{control}}) \times 100\%$$

Cellular uptake

The cellular uptake and distribution of fluorescence-labeled micelles in ARPE-19 were examined by confocal microscopy (Axiovert 100 M). One mg of FITC and 20 mg of self-assembled nanoparticles were dissolved in deionized water. This solution was added to 10 mL of deionized water, and the mixture was stirred vigorously in an ice bath for 10 min. Dialysis was performed to remove the unlabeled FITC, which were recovered by centrifugation. Subsequently, 5×10^4 cells $well^{-1}$ was seeded in a 24-well plate. After incubation, the FITC-labeled self-assembled nanoparticles were added at a concentration of 20 μg mL^{-1}. After various periods, the medium was discarded, and the cells were washed several times with PBS. The cells were fixed with 3% formaldehyde (in PBS) and washed with PBS. 0.1% Triton X-100 in PBS was added in the well for 15 min. Cells were subsequently washed three times in PBS and then stained with DAPI (1 μg mL^{-1}) solution for 1 h and rhodamine phalloidin (1 μg mL^{-1}) solution for 1 h. Finally, they were mounted on clean glass slides using mounting solution.

Results and discussion

Characterization of amphiphilic gelatin

Fig. 1(a) and (b) show the ^{1}H NMR spectra of primitive gelatin molecules and the modified one, respectively. The primitive gelatin exhibited chemical shift signals from peak 1 to peak 12, which are assigned to the protons on the primitive gelatin molecules.[13] After modifying Fig. 1(b), additional chemical signals at 0.7 ppm (CH_3), 1.1 ppm ($C_\delta H_2$), 1.2 ppm ($C_\gamma H_2$), 1.5 ppm ($C_\beta H_2$), and 2.2 ppm ($COC_\alpha H_2$) were detected and assigned to the protons from the hexanoyl group, indicating a chemical linkage of the hydrophobic hexanoyl group on the gelatin backbone. The signal at 2.8 ppm assigned to the primary amino group disappeared from its original position. The chemical shift at 3.0 ppm became broader by integral calculation. Because a chemical shift occurred at 3.2 ppm (CONH) after the substitution reaction, the spectra indicates that hydrophobic hexanoyl groups were successfully replaced by the amino protons along the gelatin molecules.

The degree of hexanoyl substitution was also determined by the TNBS reaction,[14,15] which was a method frequently employed to quantify the primary amino groups by N-trinitrophenylation of primary amine concomitant with hydrolysis of the reagent. Table 1 shows the ratio of $-NH_2$ molarity evaluated in the modified gelatin by the TNBS reaction. The content of amino groups of the modified gelatin was calculated relative to a TNBS reference containing water and primitive gelatin. It was found that the ratio of the amino group decreased with increasing substitution from GM1 to GM4. A corresponding increase in conversion as a result of the substitution was observed, which approached 100% when the hydrophobic substitution was achieved at GM4. Fig. 2 illustrates the FT-IR spectra of the modified gelatin with various hexanoyl substitutions. The original gelatin showed the bands at 1650 cm^{-1} (amide I), 1457–1542 cm^{-1} (amide II), 1235 cm^{-1} (amide III) and a weak vibration band at 2800–3000 cm^{-1}. Compared with the primitive gelatin, the modified gelatin showed a characteristic sharp peak at around 2921 cm^{-1} (CH_2, asymmetric) and 2853 cm^{-1} (CH_2, symmetric) belonging to the stretching band of the hydrophobic alkyl chains. This further substantiates the successful conjugation of hexanoyl groups with the gelatin.[16]

Self-assembly behavior

Since the hydrophobic hexanoyl groups successfully replaced part of the amino groups along the gelatin molecule, this hydrophobically modified gelatin possesses two different groups anchored along the chain, *i.e.*, hydrophobic and hydrophilic groups, imparting amphiphilicity to the modified gelatin. Such

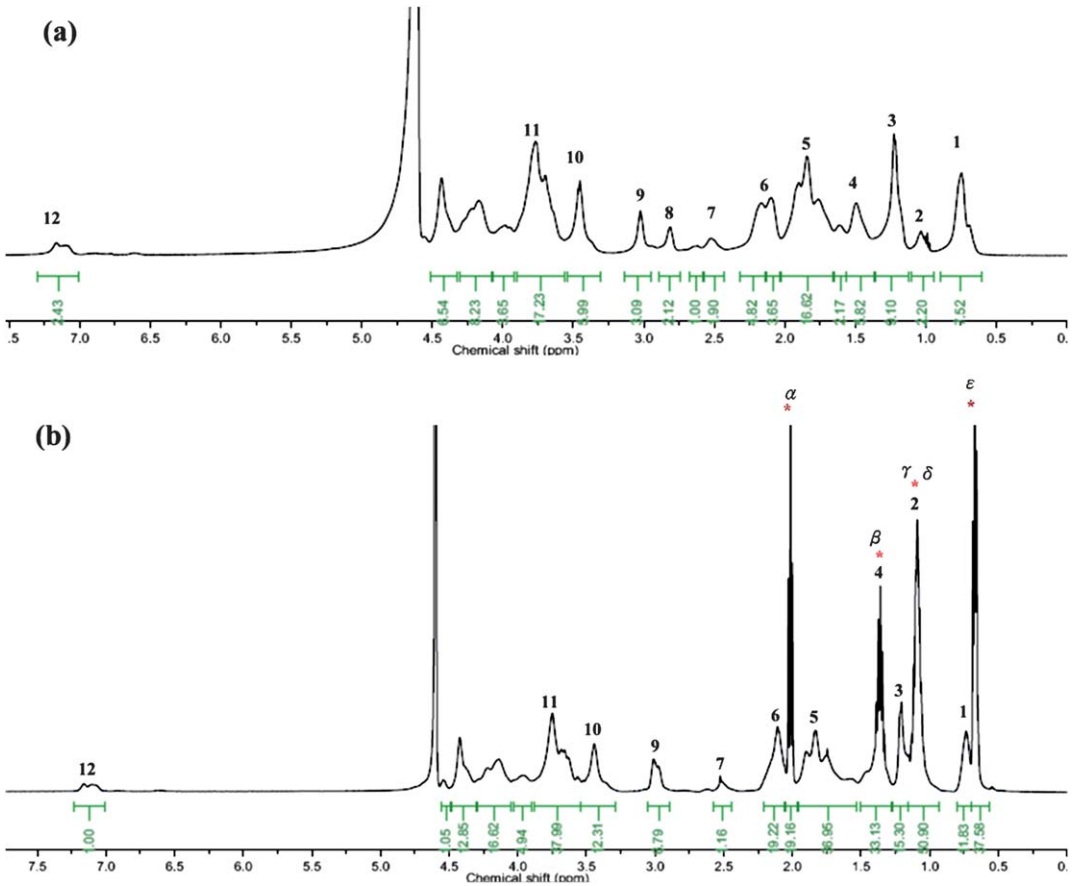

Fig. 1 ^{1}H NMR spectrum of gelatin molecules in D_2O for (a) primitive gelatin molecules and (b) gelatin derivative molecules.

an amphiphilicity renders the modified gelatin capable of undergoing conformational rearrangement upon dissolving in an aqueous environment, as observed in a number of amphiphilically modified macromolecules capable of self-assembly.[17,18] These macromolecules are then expected to form a micelle-like aggregate in aqueous solutions, and a direct observation using electron microscopy has confirmed this argument. The critical aggregation concentration (CAC) of the amphiphilic gelatin was determined by the fluorescence technique with pyrene as a fluorescence probe. As a widely used methodology, pyrene as a probe can accurately monitor the change in polarity of a given environment on a molecular scale. The transfer of pyrene from the polar environment to a non-polar region significantly changes the intensity ratio of the first peak (373 nm) and the third peak (383 nm), I_{373}/I_{383}. However, due to the difference in the local polarity, the emission spectrum of the pyrene molecule varies with the formation of the polymeric micelle as well. Hence, the critical aggregation concentration (CAC), which is defined as the threshold concentration of self-aggregate formation by intra and/or intermolecular association, can be determined from the change of the I_{373}/I_{383} value of pyrene in the presence of polymeric amphiphiles. Fig. 3 illustrates the changes of the I_{373}/I_{383} value as a function of the concentrations of various degrees of conversion of the amphiphilic gelatin. The CAC can then be determined by the intercept of two straight lines. As seen in Table 1, the CAC values decrease with the increase of hydrophobic substitution. It was found that the highest amount of substitution resulted in the lowest CAC, *i.e.*, 0.00216 mg mL^{-1}, which correlated to the solubility of the hydrophobic segments in an aqueous solution. To reduce the free energy and enhance the

Table 1 Characterization of different degrees of substitution for the self-assembled nanoparticles

Sample	Hexanoic anhydride (M)	CAC[a] ($\times 10^{-3}$ mg ml^{-1})	Mean size[b] (nm)	PDI	Zeta potential[c] (mV)	NH_2 group (%)	Conversion (%)	Encapsulation efficiency (%)
GM1	0.21	10 ± 0.38	58.4 ± 8.8	0.42 ± 0.11	−9.3 ± 1.3	30.4 ± 4.2	69.6 ± 4.2	43.1
GM2	0.42	7.08 ± 0.36	79.2 ± 8.2	0.71 ± 0.08	−11.5 ± 1.8	19.4 ± 5.5	80.6 ± 5.5	51.5
GM3	0.63	3.16 ± 0.42	105.3 ± 7.4	0.75 ± 0.10	−15.4 ± 2.0	10.2 ± 4.7	89.8 ± 4.7	60.8
GM4	0.84	2.16 ± 0.35	130.2 ± 12.8	0.52 ± 0.15	−18.2 ± 2.5	2.3 ± 2.2	97.7 ± 2.2	71.2

[a] Critical aggregation concentration determined from I_{373}/I_{383} data. [b] The size and size distribution determined by the dynamic light scattering method with three trials. [c] The zeta potential measured by a photon correlation spectrometer with three trials.

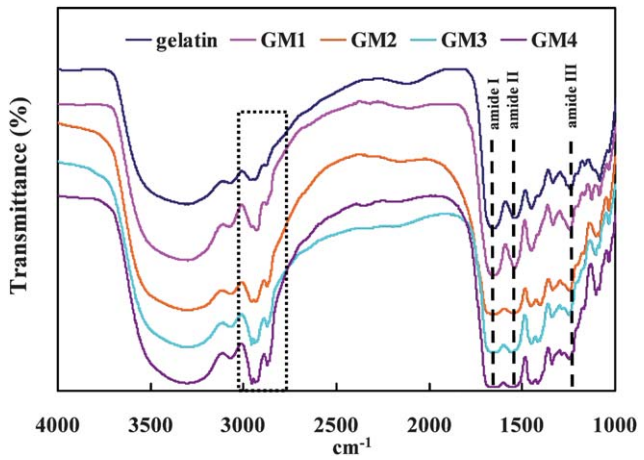

Fig. 2 The FT-IR spectra of amphiphilic gelatin molecules.

stability of the amphiphilic gelatin-water system, the hydrophobic segments along the modified gelatin would aggregate inward to form a micelle-like configuration with a hydrophobic core and a hydrophilic shell. Therefore, a high amount of substitution allowed the formation of self-assembled nanoparticles in a thermodynamically favored manner at very low CAC in aqueous solutions. Such a low CAC ensured structural stability of the nanoparticles in blood circulation.

Characterization of self-assembled nanoparticles

The surface charge of the self-assembled nanoparticles was measured by a zeta potential analyzer. Table 1 gives the zeta potentials of the nanoparticles, which are negatively charged in aqueous solution. The negatively charged surface may be due to the carboxylate groups that resided on the outer surface of the amphiphilic gelatin nanoparticles after self-aggregation in an aqueous solution. The isoelectric point of primitive gelatin was in the range of 7.0–9.0,[19] indicating a positively charged character. However, the self-assembled nanoparticles exhibited a negatively charged character. It is assumed that, as more active amino groups reacted, fewer positive charges remained, as they were

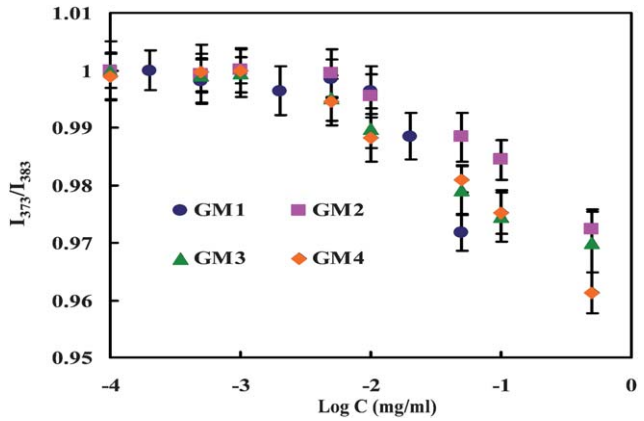

Fig. 3 Change of the intensity ratio (I_{373}/I_{383}) from excitation spectra of pyrene (5×10^{-7} mol L^{-1}) with various concentrations of amphiphilic gelatin molecules.

replaced by the hexanoyl groups. As a result, the carboxylate groups dominated the surface charge of self-assembled nanoparticles, as illustrated in Scheme 1, which resulted in a negatively charged surface. A similar argument was disclosed in the lactic acid oligomer-grafted gelatin amphiphiles.[11]

Table 1 gives the mean size of the self-assembled gelatin nanoparticles ranging from 60 to 130 nm with increased conversion effect, *i.e.*, with decreased amino residue.[20–22] It was reported in some cases that the size of amphiphilic nanoparticles decreased with increasing hydrophobic substitution. However, gelatin is a biomacromolecule that possesses steric hydrophobic amino acid residues such as isoleucine (HI 4.5), valine (HI 4.2) and leucine (HI 3.8). The hydropathy index (HI) is a normalized scale derived from the transfer of Gibbs free energy for amino acid side chains from water to vapor.[23] The value of the index ranges from −4.5 to +4.5 and describes the empirical hydrophilic and hydrophobic inclinations of a given amino acid side chain, with a negative value indicating its hydrophilic inclination. When the amphiphilic gelatin forms a micelle-like structure as a result of hydrophobic forces, its steric branch may exert an adverse effect on the aggregation size. Fig. 4 shows the morphological appearance of these nanoparticles which are relatively uniform and spherical in shape. As the hydrophobic substitution in GM4 was increased, it was found that the size of these nanoparticles increased to approximately 140 nm, Fig. 4(d). For comparison with the initial-formed structure of the GM4 nanoparticles in Fig. 4 (e), the nanoparticles immersed after 7 days in the solution were found to form a layer of gray corona approximately 10 nm. As seen in Fig. 4(f), such a corona was observed along the outer region of the nanoparticles as a relatively loose structure. This will be discussed in a forthcoming analysis and is believed to be a result of degradation.

Drug loading and release behavior

As a model molecule, the hydrophobic anti-cancer drug camptothecin (CPT) was loaded into the modified gelatin nanoparticles. As given in Table 1, the drug-loading efficiency of the nanoparticles increased with increasing hydrophobic substitution and ranged from 43.3% to 70.1%. The improved encapsulation efficiency of the self-assembled nanoparticles with hydrophobic substitutions could be due to the increase in hydrophobic interactions between the drug and modified gelatin. Fig. 5(a) shows the release profiles of CPT-loaded nanoparticles. It was found that the CPT showed a two-step release profile: a slow and linear release over a period of 8 to 12 days, depending on the degree of hexanoyl substitution, followed by a rapid release for the rest of the period. In the first-stage release, drug molecules diffused constantly from the nanoparticles due to the driving force exerted by the concentration gradient. The release rate, *i.e.*, the slope of the linear portion, appeared to decrease with increasing hydrophobic substitution, indicating a decrease in release rate with increasing hexanoyl substitution. This argument also suggests that the hydrophobic interaction between CPT molecules and hexanoyl ligands enhances the hydrophobicity of the CPT-loaded nanoparticles, and a possible dipole–dipole attraction exerted upon both hydrophobic segments of the two molecules impedes the CPT diffusion toward the eluting medium. Furthermore, the CPT release at the first stage showed

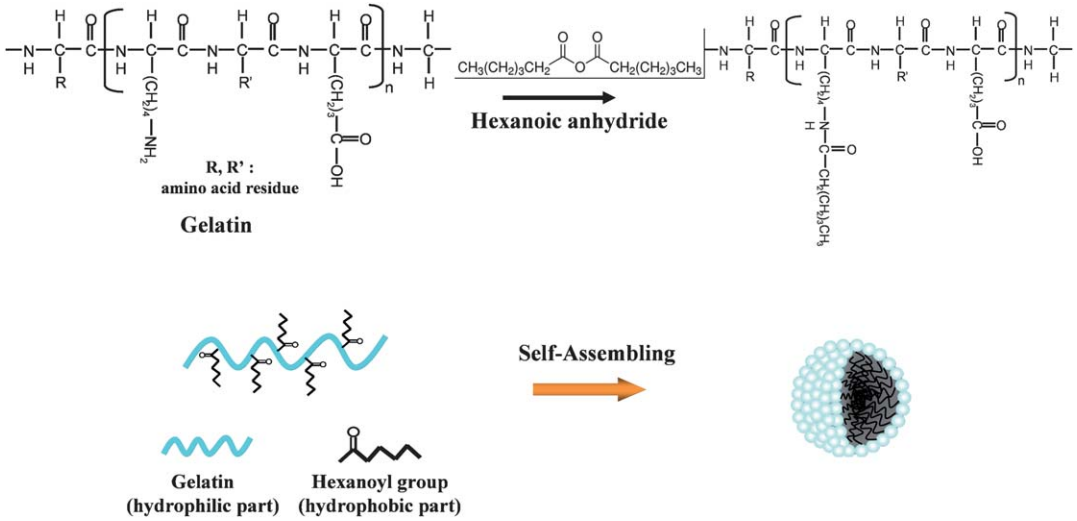

Scheme 1 The reaction scheme for the synthesis of self-assembled nanoparticles.

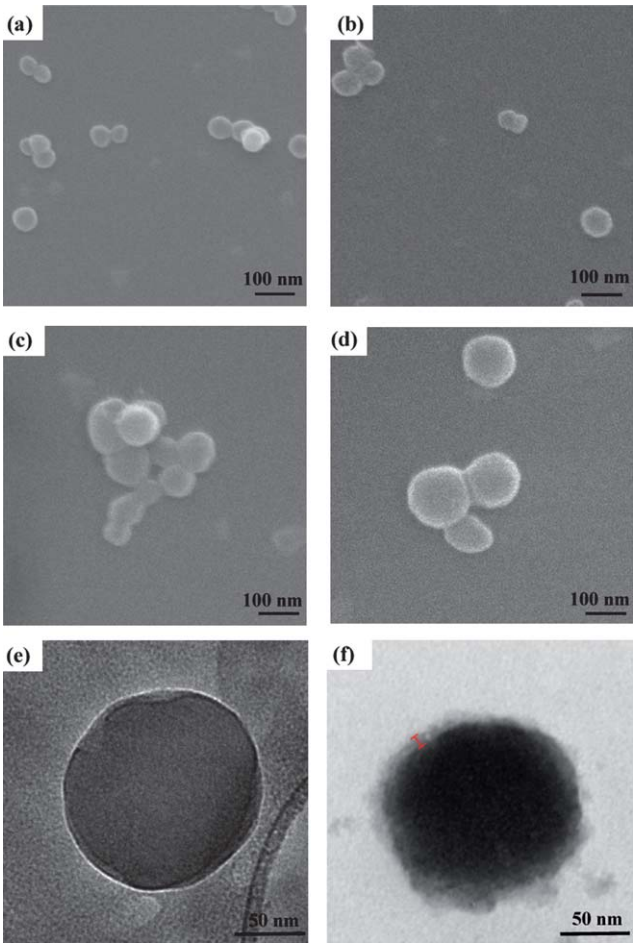

Fig. 4 Morphological appearance for the modified gelatin with different degrees of substitution for (a) GM1, (b) GM2, (c) GM3, (d) GM4; (e) and (f) are the structural evoluiton of GM4 before and after immersed in the solution for 7 days.

a linear kinetic behavior, and the slower release rate for the larger nanoparticles with higher hydrophobic substitutions suggested a longer molecular diffusion path for CPT to the releasing medium. In other words, a longer release period is required for the gelatin molecules with higher hydrophobic substitution. However, what is more interesting is that the length of eluting time duration over the linear region of the release profile increased with increasing hydrophobic substitution, from approximately 8 days to 12 days for the nanoparticles from GM1 to GM4 followed by a rapid release until day 16. One plausible explanation for the second-stage rapid release profile is due to the degradation of the modified gelatin, which may be altered from the primitive version as a result of hexanoyl substitution.[16,24] Hence, a prolonged survival of the modified gelatin nanoparticles in an aqueous solution is highly possible after hexanoyl modification. This can be evidenced indirectly from the abrupt change of their releasing profiles. For GM1, a structural disintegration can be expected at day 9, whereas the disintegration is expected at day 13 for GM4. Fig. 5(b) shows the degradation pattern of the nanoparticles. It appears that a prolonged degradation occurred with increasing hexanoyl substitution. Although the degradation behavior is somewhat similar in pattern to that of the drug release profile, the length of time scale between two profiles is different. The degradation profiles illustrated a 2-stage pattern, starting with a slow profile followed by rapid degradation. When compared with the release profiles in Fig. 5(a), the drug release profile was very similar to the degradation profile, especially at the second-stage region. As mentioned above, we believe that the hydrophobic interaction as a result of CPT incorporation may contribute to a two-fold effect: (1) increasing the water-repelling property of the resulting CPT-loaded nanoparticles and (2) enhancing the intermolecular forces between the hexanoyl groups along the amphiphilic gelatin chain, making it less water-soluble. Both factors may explain (1) the slow and linear first-stage release, because the CPT movement is largely hindered by intermolecular interactions and a delay in degradation compared to the primitive gelatin. The rapid second-stage release was due to the modified gelatin subjected to extensive degradation. In other words, the first-stage release of the CPT is diffusion-dominated, while the second-stage release is degradation-dominated. This argument can be directly evidenced in Fig. 6(a) and (b), in which the morphology of the nanoparticles in GM1 demonstrated a diffused

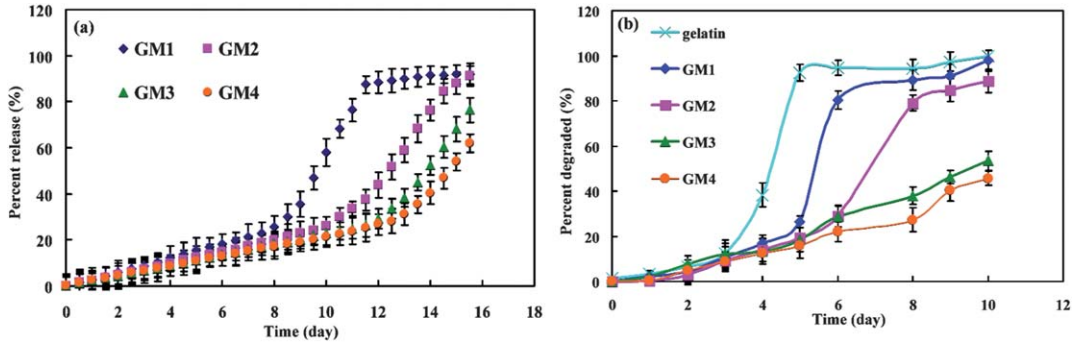

Fig. 5 (a) CPT release profiles for the different degrees of substitution of self-assembled nanocarriers. (b) Degraded profiles for the different degrees of substitution of self-assembled nanocarriers.

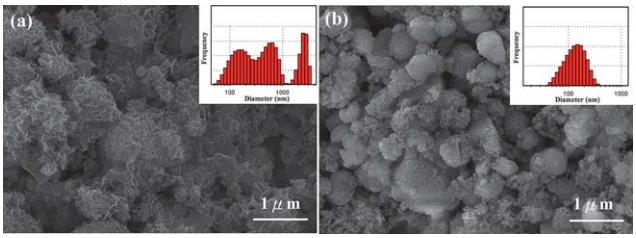

Fig. 6 CPT loaded self-assembled gelatin nanoparticles after 12 days at different substitution for (a) GM1 and (b) GM4.

structure at day 9, whereas the morphology remained the same for GM4 because the primitive gelatin is soluble and degradable in an aqueous solution. The study demonstrated that drug elution from the modified gelatin nanoparticles with a variety of hexanoyl substitutions followed a combination of both diffusion-controlled and erosion-controlled mechanisms.[25] Therefore, controlled CPT release can be easily achieved by fine-tuning of the number of hexanoyl ligands along the primitive gelatin macromolecule. This finding enables the development of a new type of amphiphilic protein-like nanoparticles for drug delivery applications.

Cell viability

To explore the potential for drug delivery uses, the cytocompatibility of the nanoparticles were further investigated using human retinal pigmented epithelium cells (ARPE-19), as shown in Fig. 7. The cell viability of the modified gelatin nanoparticles was investigated using the MTT assay, which has long been a popular method to evaluate cytocompatibility. Fig. 7(a) shows the cell viability after 24 h incubation with the nanoparticles at various concentrations between 1 μg mL^{-1} and 1000 μg mL^{-1}. The results demonstrate that ARPE-19 cells cultured with nanoparticles over the entire range of concentrations remained highly viable compared to the control group. In other words, these gelatin-based nanoparticles exhibited excellent biocompatibility and relatively low cytotoxicity to the ARPE-19 cells. Fig. 7(b) shows the cell viability after 24, 48, and 72 h incubation with the nanoparticles that have various hexanoyl substitutions. The cell viability of ARPE-19 cells cultured with the nanoparticles was not significantly affected for as long as 72 h. These observations proved the compatibility of the hexanoyl modification and showed the suitability of the resulting nanoparticles for medical uses.

Cellular uptake

Cellular uptake of the FITC-labeled self-assembled nanoparticles was investigated by an Axiovert 100 M confocal microscope. After 24 h of ARPE-19 cell incubation, which is employed as a normal cell model, cells treated with FITC-labeled self-assembled nanoparticles for various time durations were monitored. Fig. 8 shows that the nanoparticles subjected to the cells with an exposure time period varying from 30 min to 4 h

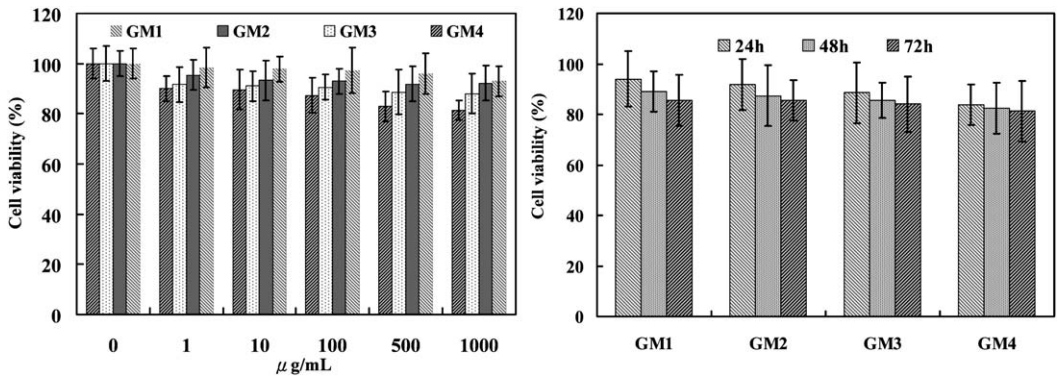

Fig. 7 (a) Cell viability of ARPE-19 cells after 24 h of incubation with increasing amounts of self-assembly nanoparticles (b) Cell viability of ARPE-19 cells after 24 to 72 h of incubation with the same amounts (500 μg ml^{-1}) of self-assembly nanoparticles. Cell viability was measured using an MTT assay.

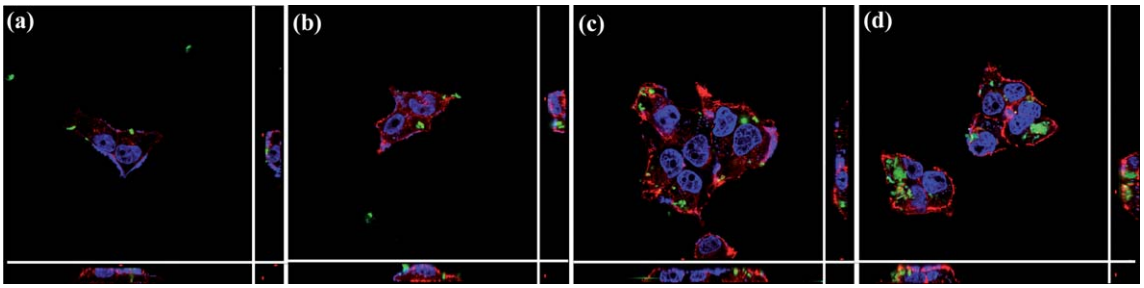

Fig. 8 Time-course PL microscopy images of ARPE-19 cells labeled with FITC-loaded self-assembled nanoparticles. The cell skeleton was stained with rhodamine phalloidin (red), and the cell nucleus was stained with DAPI (purple). Cells were incubated with FITC-loaded self-assembled nanoparticles for (a) 30 min (b) 1 h (c) 2 h and (d) 4 h.

were gradually taken up by the cells, possibly through endocytosis. For an incubation time of 30 min, only a few nanoparticles appeared on the surface of the cell membranes. The number of nanoparticles further increased after 1 h incubation, showing that the FITC-labeled self-assembled nanoparticles attached onto the cell membrane with some migrated to the cytoplasm region, as indicated by some light spots clearly visible in the cytoplasm regions. After 4 h of incubation, considerable regions of the cytoplasm displayed strong green fluorescence, indicating that the nanoparticles were efficiently internalized and localized within the cells. This preliminary finding confirmed the cytocompatibility and rapid internalization of the amphiphilic gelatin nanoparticles, over which a vast number of biomedical applications, such as intracellular drug delivery medication, can be expected.

Conclusion

In present study, we demonstrated the use of a facile chemical method to synthesize amphiphilic gelatin capable of self-assembling into micelle-like nanospheres. The particle size, surface charge, and CAC of the self-assembled nanoparticles with different degrees of hexanoyl substitution were systematically investigated. SEM and TEM examination proved the self-assembly capability of the resulting hexanoyl-modified gelatin molecules, forming spherical nanoobjects. The negative surface charge upon hexanoyl substitution ensures the colloidal stability of the nanoparticles, and in the meantime, renders a chemically and biologically benign property towards cells. Drug release can be well-tuned *via* the degree of hexanoyl substitution and these new protein-based nanoparticles permit an intracellular nanotherapy effectively operated for anti-cancer purposes.

Acknowledgements

This work was financially supported by the National Science Council of the Republic of China, Taiwan, under Contracts NSC98-2627-B-009-001, NSC-98-3114-E-009-006 and NSC 99-2113-M-009-013-MY2.

References

1 K. Park, S. Lee, E. Kang, K. Kim, K. Choi and I. C. Kwon, *Adv. Funct. Mater.*, 2009, **19**(10), 1553–1566.
2 F. Y. Cheng, S. P. H. Wang, C. H. Su, T. L. Tsai, P. C. Wu, D. B. Shieh, J. H. Chen, P. C. H. Hsieh and C. S. Yeh, *Biomaterials*, 2008, **29**(13), 2104–2112.
3 M. Elsabahy, N. Wazen, N. Bayo-Puxan, G. Deleavey, M. Servant, M. J. Damha and J. C. Leroux, *Adv. Funct. Mater.*, 2009, **19**(24), 3862–3867.
4 B. D. Chithrani and W. C. W. Chan, *Nano Lett.*, 2007, **7**(6), 1542–1550.
5 C. B. Carlson, P. Mowery, R. M. Owen, E. C. Dykhuizen and L. L. Kiessling, *ACS Chem. Biol.*, 2007, **2**(2), 119–127.
6 F. X. Gu, R. Karnik, A. Z. Wang, F. Alexis, E. Levy-Nissenbaum, S. Hong, R. S. Langer and O. C. Farokhzad, *Nano Today*, 2007, **2**(3), 14–21.
7 S. Y. Fung, J. Duhamel and P. Chen, *J. Phys. Chem. A*, 2006, **110**(40), 11446–11454.
8 Z. G. Hu, X. S. Fan, H. J. Wang and J. J. Wang, *Polymer*, 2009, **50**(17), 4175–4181.
9 C. C. Huang, C. H. Su, W. M. Li, T. Y. Liu, J. H. Chen and C. S. Yeh, *Adv. Funct. Mater.*, 2009, **19**(2), 249–258.
10 S. Kamiya, M. Yamada, T. Kurita, A. Miyagishima, M. Arakawa and T. Sonobe, *Int. J. Pharm.*, 2008, **354**(1–2), 242–247.
11 T. Tanigo, R. Takaoka and Y. Tabata, *J. Controlled Release*, **143**(2), 201–206.
12 U. Salma, N. Chen, D. L. Richter, P. B. Filson, B. Dawson-Andoh, L. Matuana and P. Heiden, *Macromol. Mater. Eng.*, **295**(5), 442–450.
13 V. V. Rodin and V. N. Izmailova, *Colloids Surf., A*, 1996, **106**(2–3), 95–102.
14 Y. W. Won and Y. H. Kim, *J. Controlled Release*, 2008, **127**(2), 154–161.
15 O. Toledano and S. Magdassi, *J. Colloid Interface Sci.*, 1997, **193**(2), 172–177.
16 L. H. Lin and K. M. Chen, *Colloids Surf., A*, 2006, **272**(1–2), 8–14.
17 C. Keyes-Baig, J. Duhamel, S. Y. Fung, J. Bezaire and P. Chen, *J. Am. Chem. Soc.*, 2004, **126**(24), 7522–7532.
18 S. Y. Fung, H. Yang and P. Chen, *Colloids Surf., B*, 2007, **55**(2), 200–211.
19 A. Saxena, K. Sachin, H. B. Bohidar and A. K. Verma, *Colloids Surf., B*, 2005, **45**(1), 42–48.
20 C. T. Lee, C. P. Huang and Y. D. Lee, *Biomacromolecules*, 2006, **7**(4), 1179–1186.
21 K. H. Liu, S. Y. Chen, D. M. Liu and T. Y. Liu, *Macromolecules*, 2008, **41**(17), 6511–6516.
22 C. X. Guo, S. Q. Liu, Z. F. Dai, C. Jiang and W. Y. Li, *Colloids Surf., B*, 2010, **76**(1), 362–365.
23 J. Kyte and R. F. Doolittle, *J. Mol. Biol.*, 1982, **157**(1), 105–132.
24 L. Y. Chen, G. Remondetto, M. Rouabhia and M. Subirade, *Biomaterials*, 2008, **29**(27), 3750–3756.
25 A. Gopferich, *Biomaterials*, 1996, **17**(2), 103–114.

